The photodissociation dynamics of OCS at 248 nm: The S(^3P_J) atomic angular momentum polarization

M. Brouard,[a] F. Quadrini, and C. Vallance
The Physical and Theoretical Chemistry Laboratory, The Department of Chemistry, University of Oxford, South Parks Road, Oxford OX1 3QZ, United Kingdom

(Received 16 May 2007; accepted 19 June 2007; published online 23 August 2007)

The dissociation of OCS has been investigated subsequent to excitation at 248 nm using velocity map ion imaging. Speed distributions, speed dependent translational anisotropy parameters, and the atomic angular momentum orientation and alignment are reported for the channel leading to S(^3P_J). The speed distributions and β parameters are in broad agreement with previous work and show behavior that is highly sensitive to the S-atom spin-orbit state. The data are shown to be consistent with the operation of at least two triplet production mechanisms. Interpretation of the angular momentum polarization data in terms of an adiabatic picture has been used to help identify a likely dissociation pathway for the majority of the S(^3P_J) products, which strongly favors production of $J=2$ fragment atoms, correlated, it is proposed, with rotationally hot and vibrationally cold CO cofragments. For these fragments, optical excitation to the $2\,^1A'$ surface is thought to constitute the first step, as for the singlet dissociation channel. This is followed by crossing, via a conical intersection, to the ground $1\,^1A'$ state, from where intersystem crossing occurs, populating the $1\,^3A'/1\,^3A''(^3\Pi)$ states. The proposed mechanism provides a qualitative rationale for the observed spin-orbit populations, as well as the S(^3P_J) quantum yield and angular momentum polarization. At least one other production mechanism, leading to a more statistical S-atom spin-orbit state distribution and rotationally cold, vibrationally hot CO cofragments, is thought to involve direct excitation to either the $^3\Sigma^-$ or $^3\Pi$ states. © *2007 American Institute of Physics*.
[DOI: 10.1063/1.2757619]

I. INTRODUCTION

In the following paper we discuss the dynamics of the spin-forbidden channel arising from the photodissociation of carbonyl sulphide (OCS) at 248 nm,

$$\mathrm{OCS} + h\nu \rightarrow \mathrm{CO}(X\,^1\Sigma^+) + \mathrm{S}(^3P_J), \quad \lambda < 388\ \mathrm{nm}. \qquad (1)$$

Compared with the singlet channel, leading to S($^1D_2$) +CO($X\,^1\Sigma^+$), which was the subject of the preceding paper,[1] there have been comparatively few studies of process (1). Much of the early theoretical effort towards calculating potential energy surfaces for this system was concerned with the lowest singlet and triplet states involved in the electronic quenching of singlet S atoms by CO (Refs. 2–6) via the processes

$$\mathrm{S}(^1D) + \mathrm{CO}(^1\Sigma^+) \rightarrow \mathrm{S}(^3P) + \mathrm{CO}(^1\Sigma^+; v, J), \qquad (2)$$

$$\mathrm{O}(^1D) + \mathrm{CS}(^1\Sigma^+) \rightarrow \mathrm{S}(^3P) + \mathrm{CO}(^1\Sigma^+; v, J). \qquad (3)$$

Three electronic states of OCS correlate with the triplet product channel: the $1\,^3A'$ and $1\,^3A''$ Renner-Teller pair ($^3\Pi$ at linearity) and the $2\,^3A''(^3\Sigma^-)$ state. The latter has not been characterized theoretically. One dimensional slices through these potentials at linearity are shown schematically in Fig. 1. Note that the energy ordering of these states, $1\,^3A'' \sim 1\,^3A' < 2\,^3A''$, is expected on the basis of orbital occupation at linearity,[2] in which the p_z orbital (aligned along the bond axis) is doubly occupied in the case of the $2\,^3A''(^3\Sigma^-)$ state, but only singly occupied in the case of the $1\,^3A'$ and $1\,^3A''$ states.

Inagaki *et al.* combined experimental measurements[3] of the rovibrational distribution of CO($X\,^1\Sigma^+$) fragments following collisions with S($^1D_2$) atoms, with quasiclassical trajectory calculations on a series of London-Eyring-Polanyi-Satu surfaces to study process (2). Two main mechanisms were identified: (a) a direct conversion through intersystem crossing at the crossing between singlet and triplet surfaces and (b) a mechanism involving a long lived complex residing in the well of the ground singlet surface. Good agreement between predicted and measured rovibrational distributions indicated that the mechanism involving a complex intermediate plays an important role. Tachikawa[4] and Tachikawa *et al.*[5] extended the theoretical treatment by including spin-orbit coupling and investigating the collision energy dependence of the dynamics for collinear geometries. A third mechanism was identified, in which the trajectories first crossed onto the triplet surface, as in the direct mechanism, but subsequently recrossed back onto the singlet state, and were found to reside in the singlet potential well before finally recrossing to form the triplet products. The mechanism involving the complex intermediate identified by Inagaki *et al.* was shown to be dominant at all collision energies

[a]Electronic mail: mark.brouard@chem.ox.ac.uk

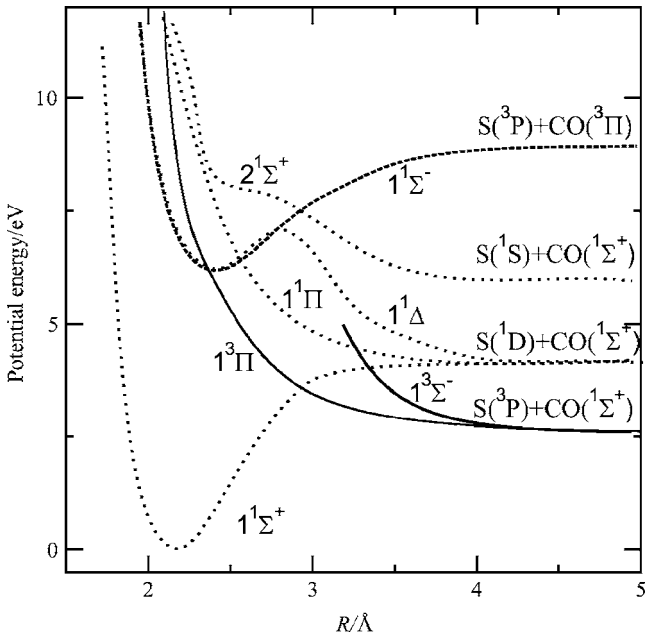

FIG. 1. Schematic representation of the triplet (——) and singlet (·····) potential energy curves for OCS as a function of Jacobi coordinate R at a linear OCS configuration. The location of the $1\,^3\Pi$ surface is taken from Ref. 3, while the $1\,^3\Sigma^-$ surface has not yet been calculated, and its location is thus more speculative. The singlet surfaces are adapted from those of Ref. 11.

investigated,[5] although the contribution to the dynamics of the direct mechanism was seen to increase with collision energy.

The first direct measurements of the $S(^3P_J)$ yield following photoexcitation were by Houston and co-workers, who estimated a maximum quantum yield of 2%.[7,8] This estimate was later revised by Nan *et al.*[9] to be around 5%. In their work, Nan *et al.* measured Doppler-resolved laser induced fluorescence profiles for the $S(^3P_2)$ atoms produced from the photodissociation of OCS at 222 nm. The authors found an isotropic contribution to the signal due to $S(^1D_2)$ relaxation needed to be taken into account to fit the data accurately. The nascent speed distribution thus recorded indicated that a large degree of excess energy was released into cofragment internal excitation (60%). A speed averaged value of $\beta = 0.3 \pm 0.2$ was reported.

The ion imaging technique was used by Suzuki and co-workers to investigate the nascent distribution of $S(^3P_2)$ fragments[10] and later all three spin-orbit states[11] following 223 nm dissociation. Their reported speed distributions were in agreement with previous measurements.[9] The speed resolution afforded by the two-dimensional imaging technique allowed Suzuki and co-workers to identify two speed regimes[11] reminiscent of findings for the singlet channel discussed in the preceding paper.[1] Speed averaged β parameters were reported for the two regimes: $\beta_s = 1.1$ and $\beta_f = 0.2$ for $S(^3P_2)$. Values for the other spin-orbit states were not reported but appear to be positive based on the raw images shown in Ref. 11. The speed distributions reported were found to vary noticeably with S-atom spin-orbit state.

In high resolution imaging studies of the CO products following irradiation at 230 nm, Sugita *et al.* reported the appearance of rings in images for CO $J \gtrsim 65$ that could be ascribed on energetic grounds to triplet channel dissociation.[12] This result indicated that, for some fragments, a high proportion of the excess energy (which is greater for the triplet channel than the singlet), must be deposited into CO rotational excitation. The authors suggested that this phenomenon indicated that triplet states are only accessed from highly bent geometries. In recent experiments by Lipcinc and Janssen, the greater resolution afforded by the implementation of slice imaging[13] allowed better separation of rings arising from hot band dissociation and triplet channel dissociation. The triplet quantum yield was found to be smaller than those determined from quantum-state averaged measurements, the reported value being 0.038 for $OCS(v_2 = 0)$.

In the following paper we report a detailed velocity map ion imaging study of the $S(^3P_J)$ photofragments generated by the photolysis of OCS at 248 nm. In the next section we briefly outline some of the experimental and data analysis procedures specific to the present study. In Sec. III we present $S(^3P_J)$ spin-orbit state populations, state-resolved speed distributions, and translational anisotropy parameters, as well as a comprehensive set of electronic angular momentum polarization data. These results provide the first complete characterization of this channel at any photodissociation wavelength. The findings are discussed in Sec. IV in the light of previous work and of simple models of the dissociation mechanisms. Comparisons are also made with the spin-forbidden channel in the photodissociation of the isovalent N_2O molecule.

II. EXPERIMENTAL AND ANALYSIS PROCEDURES

The experiments were carried out using a standard velocity map[14] ion imaging[15] apparatus that has been described in detail previously.[16–20] Each spin-orbit state was individually probed via resonantly enhanced multiphoton ionization (REMPI) using the $^3P_2 \leftarrow {}^3P_0$ transition at 311 nm, the $^3P_2 \leftarrow {}^3P_1$ transition at 310 nm, and the $^3P_1 \leftarrow {}^3P_2$ transition at 308 nm.[21] Images were collected using the same eight pump-probe polarization geometries described in Ref. 1. A small amount of nonresonant background signal at the probe wavelengths was observed. This was accounted for using a four channel data acquisition procedure, which allowed the signal obtained with only the probe laser firing to be recorded on alternate laser shots. The latter signal was then subtracted from the resonant pump-probe signal prior to fitting.

The analysis of angular momentum polarization effects by fitting Fourier moments of the ion images[16] has been described in detail previously.[22] The fitting procedure used here was identical to that described in the preceding paper.[1] The line strengths for the REMPI probe transitions, which are necessary to analyze the data for angular momentum polarization effects, were calculated using the expressions given in Refs. 23 and 24. For the present experiments, a higher number of Gaussian (35) and Legendre polynomial basis functions (9) had to be used in order to satisfactorily fit the highly structured Fourier moments recovered from the experimental images.

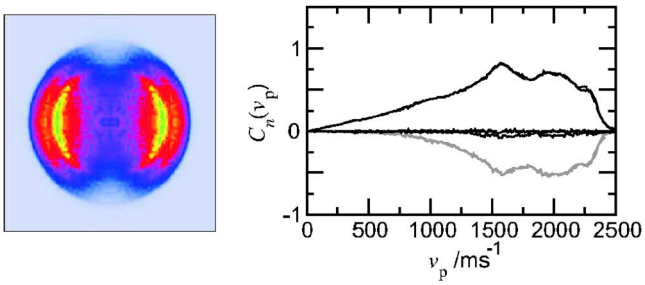

FIG. 2. (Color online) Image, Fourier moments (——) and fits (---) for S($^3P_0$) products for the HH pump-probe geometry. Nonzero experimental and fitted C_2 moments are shown in gray.

III. RESULTS

A selection of the images collected for each of the spin-orbit states are displayed in Figs. 2–4. S($^3P_0$) atoms do not posses total electronic angular momentum, and the scattering dynamics are fully parametrized by a speed distribution and $\beta(v)$. Thus, only one set of images, for which both pump and probe lasers are polarized in the plane of the image, are necessary to fully characterize this system. The image collected with this pump-probe geometry is shown in Fig. 2. Eight pump-probe geometries were selected to characterize the polarization parameters in the case of S($^3P_1$) and S($^3P_2$). For both transitions, negligible differences were observed between images (not shown) collected with alternating left and right circularly polarized probe light, indicating that the orientation parameters are near zero for these products. Nonetheless, these orientation-sensitive geometries also contain alignment contributions and, therefore, were included in the fit to provide more constraints on the fitted parameters.

While for S($^3P_1$) the maximum rank parameters are those with $K=2$, the S($^3P_2$) products could be characterized

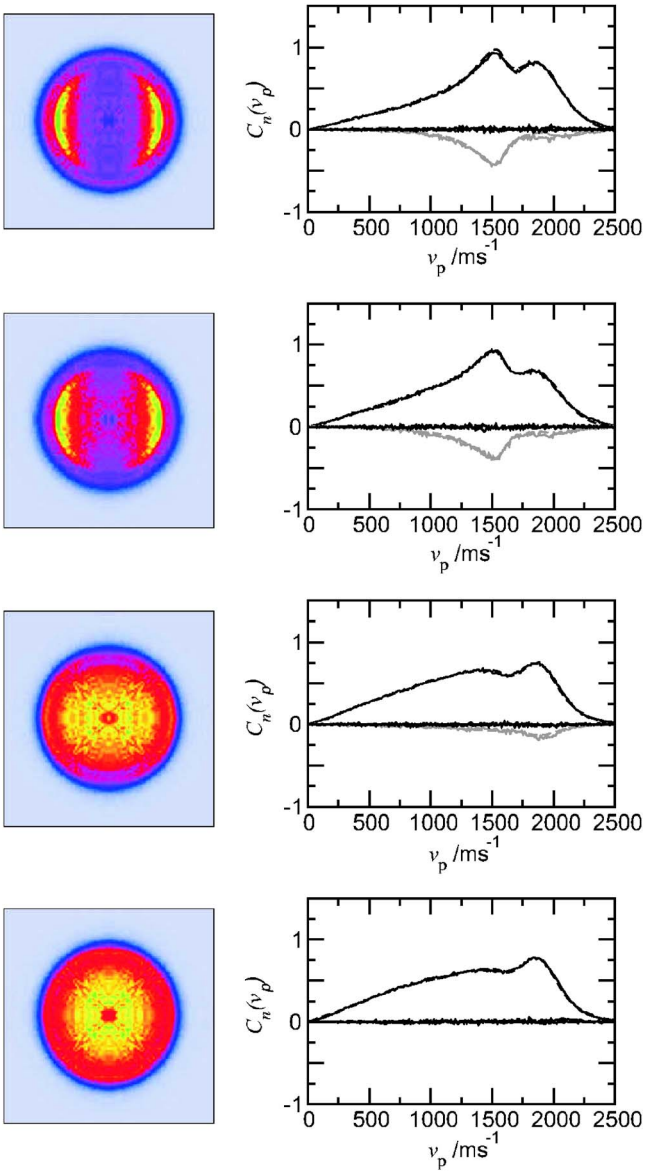

FIG. 3. (Color online) Images in false gray scale, Fourier moments (——) and fits (---) for S($^3P_1$) products. Pump-probe geometries, from top to bottom: HH, HV, VH, and VV. Nonzero experimental and fitted C_2 moments are shown in gray.

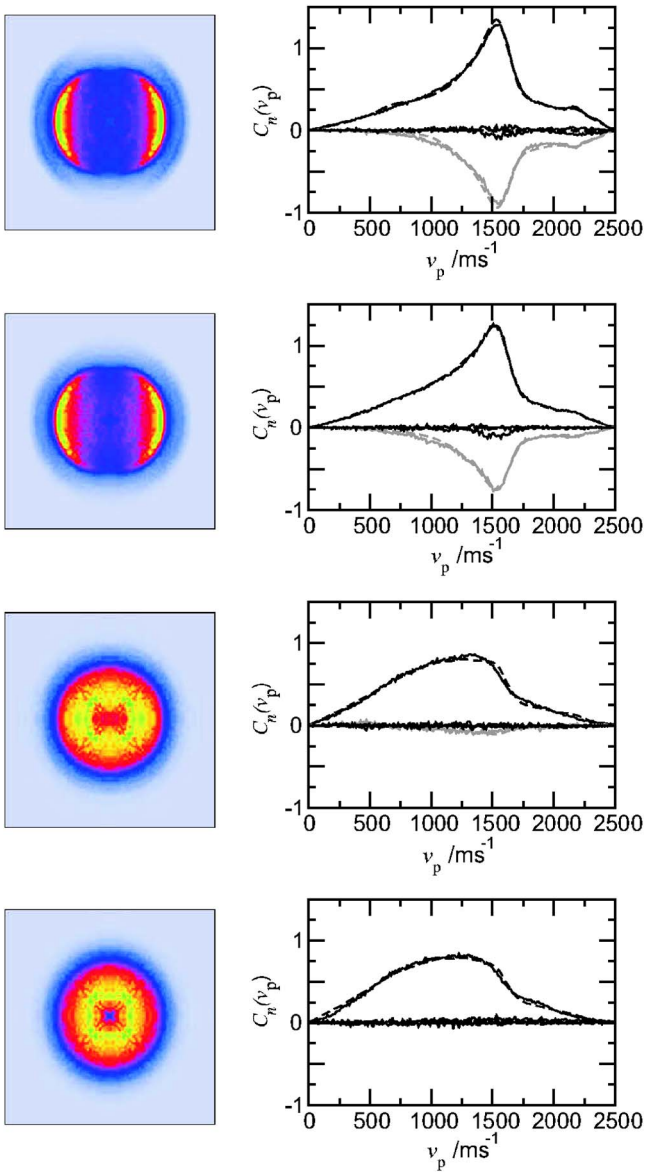

FIG. 4. (Color online) Images in false gray scale, Fourier moments (——) and fits (---) for S($^3P_2$) products. Pump-probe geometries, from top to bottom: HH, HV, VH, and VV. Nonzero experimental and fitted C_2 moments are shown in gray.

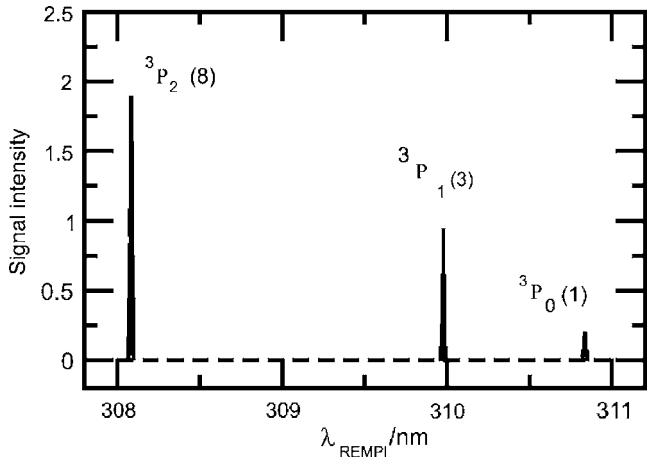

FIG. 5. REMPI scan showing relative intensity of signal arising from different spin-orbit states. Scans were collected for individual states and power normalized. Spin-orbit state assignments are given with relative integrated signal intensities displayed in brackets. As described in the text, based on the work of Refs. [26–28], the relative line strengths for detection of the different spin-orbit states of $S(^3P_J)$ were estimated to be approximately the same. The spin-orbit state populations were thus found to be $S(^3P_2):S(^3P_1):S(^3P_0)=8:3:1$.

by parameters of up to rank $K=4$. Note that, unlike for $O(^3P_2)$,[25] the P_4 line strength for $S(^3P_2)$ is not zero.[23,24] However, inspection of the images displayed in Fig. 4 indicates that $K=4$ parameters are negligible in the present system, as demonstrated by the near-zero fourth and sixth order (C_4 and C_6) Fourier moments observed in HH and VH pump-probe geometries, respectively (where XX refers to the direction of linear polarized pump and probe radiation, respectively, with H being linear polarization in the plane of the detector, and V polarization perpendicular to the plane of the detector). When the moments were fitted, the returned $K=4$ parameters were close to zero, within experimental error, and excluding them from the fit did not significantly influence the values of the other returned parameters or significantly alter the best-fit values of χ^2. As a result, $K=4$ parameters were assumed to be zero in the following analysis. Note, finally, that the line strength factor for the $K=3$ moments for the transition used to probe the $S(^3P_2)$ fragments is zero, and therefore it is also safe to neglect these moments in the analysis.

REMPI scans, in which the total ion signal was recorded as a function of wavelength, were also performed to determine the relative spin-orbit population for this channel, as illustrated in Fig. 5. Relative (2+1) REMPI line strengths for the transitions used to probe the three spin-orbit states are not known. However, conversion of signal intensity to spin-orbit populations was possible by comparison with the work of Hsu *et al.*[26] In their work, Hsu *et al.* presented REMPI spectra for $S(^3P_J)$ products from the dissociation of CS_2 at 193 nm, using the same probe transitions as here (given in Sec. II). As the spin-orbit state distribution for this system is known,[27,28] the authors were able to use the above experiment as a calibration. From their work, it can be estimated that the relative line strengths for the detection of the different spin-orbit states of $S(^3P_J)$ are approximately the same. The spin-orbit state populations were thus estimated here to be $S(^3P_2):S(^3P_1):S(^3P_0)=8:3:1$.

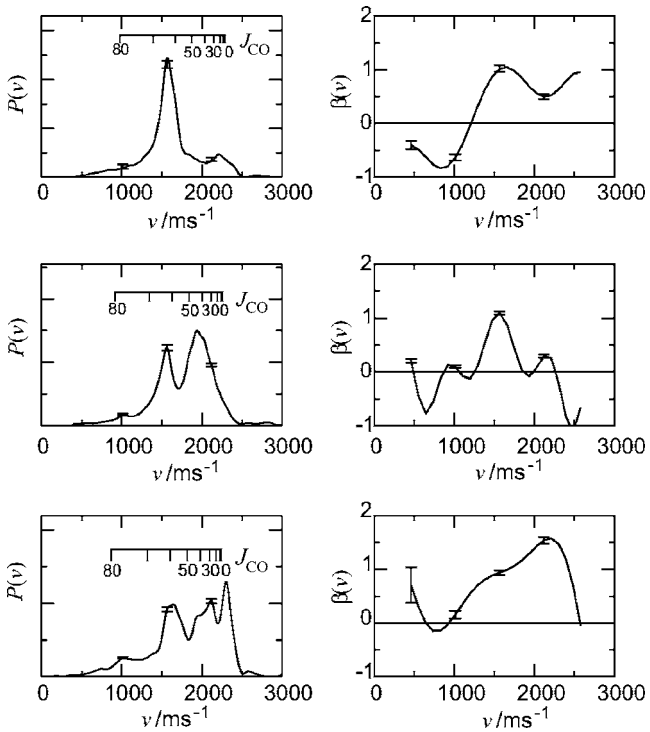

FIG. 6. Speed distributions and $\beta(v)$ parameters for (from top to bottom) $S(^3P_2)$, $S(^3P_1)$, and $S(^3P_0)$. The combs show the positions of the rotational states of the CO cofragment in $v=0$, calculated assuming that excitation occurs from the vibrational ground state of OCS (see text for details).

The returned speed distributions and $\beta(v)$ parameters for the three spin-orbit states are displayed in Fig. 6. Speed dependent alignment parameters for $S(^3P_1)$ and $S(^3P_2)$ are shown in Fig. 7, while in Table I we present the velocity-averaged anisotropy and polarization parameters. Because the speed distributions for the three spin-orbit states of sulphur are so structured, we also break the velocity-averaged data down into a number of distinct features discussed further in the following section. As noted above all of the orientation parameters were found to be zero, indicating that the total angular momentum $\boldsymbol{J}$ is aligned, but not oriented. All of the $K=2$ parameters are found to be nonzero, with particularly large contributions from γ_2, indicating some contribu-

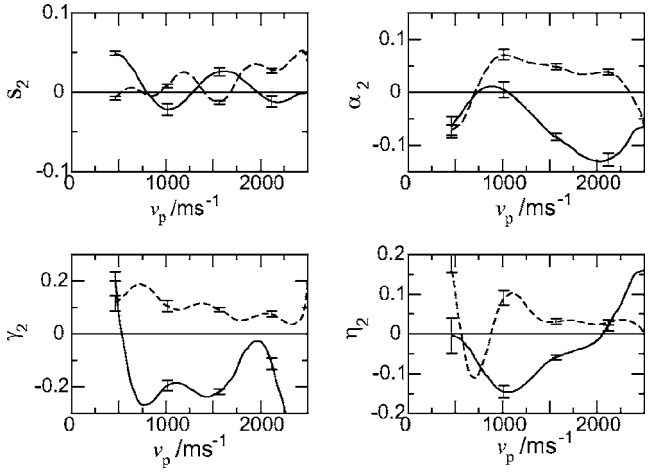

FIG. 7. Speed dependent angular momentum alignment parameters returned from fits for the $S(^3P_2)$ (——) and $S(^3P_1)$ (---) products.

TABLE I. Polarization parameters for S($^3P_2$) and S($^3P_1$). The column labeled "avg" gives the polarization parameters averaged over all speeds. The other columns give values for specific speed regimes, such as that centered around ~1580 m s^{-1}, or for all speeds apart from the 1580 m s^{-1} component (labeled "other"). The errors (1σ) are given in parentheses and refer to errors in the final digits reported.

	$^3P_2$			$^3P_1$			$^3P_0$			
	Avg	~1580	Other	Avg	~1580	Other	Avg	~1660	~2120	~2300
β	0.775(10)	0.93(6)	0.06(1)	0.318(8)	0.83(3)	0.06(1)	1.089(30)	1.00(4)	1.43 (6)	1.40(6)
α_1	−0.000(1)			−0.001(1)						
γ_1	−0.003(6)			0.000(1)						
γ_1'	−0.002(3)			−0.001(1)						
s_2	0.004(10)	0.016(5)	−0.001(3)	0.018(1)	−0.003(2)	0.028(3)				
α_2	−0.087(4)	−0.096(6)	−0.074(14)	0.038(4)	0.050(6)	0.034(5)				
γ_2	−0.173(16)	−0.160(18)	−0.189(20)	0.081(6)	0.095(9)	0.077(8)				
η_2	−0.047(5)	−0.059(6)	−0.029(4)	0.031(4)	0.036(7)	0.031(7)				

tion from alignment of $\boldsymbol{J}$ at 45° to the quantization axis (−45° in the case of $J=2$ and +45° in the case of $J=1$). The values of s_2 and α_2, which characterize the diagonal elements of the density matrix, indicate that S($^3P_2$) fragments are aligned preferentially along the z axis, while the S($^3P_1$) products have $\boldsymbol{J}$ preferentially polarized in the xy plane. Plots of the M_J populations, and of the full molecular frame atomic angular momentum distributions of $\boldsymbol{J}$,[29,30] are shown in Fig. 8.

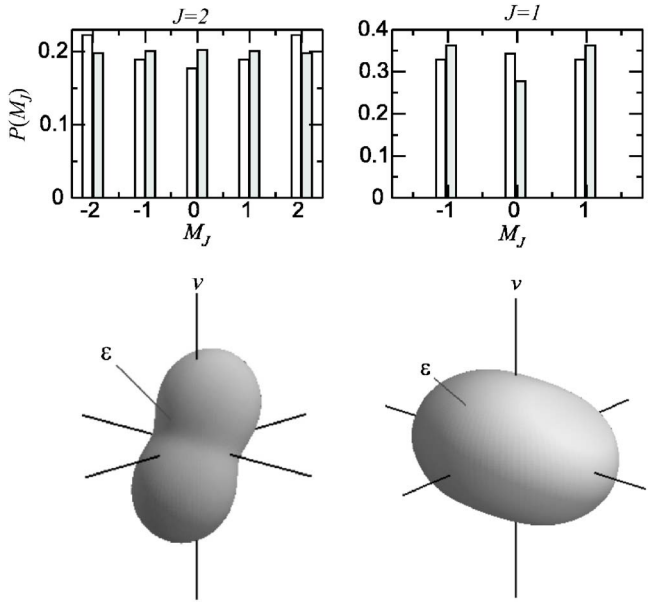

FIG. 8. Top panels: The M_J populations for the S-atom products born in $J=2$ (left panel) and $J=1$ (right panel). The open bars refer to those products born around 1580 m s^{-1}, while the shaded bars are for products born at all other speeds. Bottom panels: The molecular frame three dimensional [quantum-mechanical (Refs. 29 and 30)] distributions of $\boldsymbol{J}$ for the S($^3P_2$) (left) and S($^3P_1$) (right) atomic products traveling at ~1580 m s^{-1}. The plots are generated according to equations given in Refs. [18,19,22,48]. $\mathbf{v}$ labels the molecular frame z axis, and the zx plane contains both $\mathbf{v}$ and $\boldsymbol{\epsilon}$, the electric vector of the dissociating light, which is assumed here to be linearly polarized. Although the angular distributions will vary significantly with scattering angle between $\mathbf{v}$ and $\boldsymbol{\epsilon}$, the angle shown in the figures has been chosen to be 45°, which is reasonably close to the most probable scattering angle for the positive but nonlimiting values of β observed experimentally (see Table I). The significant tilt of these distributions away from the z axis and into the zx (left) or zy (right) planes reflects the large contributions from moments with $Q=1$ and $Q=2$, respectively. These moments do not contribute to the M_J population distributions shown in the top panels.

IV. DISCUSSION

A. Speed distributions, β parameters, and spin-orbit populations

The speed distributions and translational anisotropy shown in Fig. 6 display significant differences between the three spin-orbit states. This is striking because the excess energy available at this wavelength (nearly 15 000 cm^{-1} for the $J=2$ fragments) is much greater than the spin-orbit splitting between the atomic states (~200 cm^{-1}). Even from the raw images themselves, three rings can be identified for S($^3P_2$) and S($^3P_1$), corresponding to peaks observed in the velocity distribution shown in Fig. 6, while four rings are clearly visible in the images collected for S($^3P_0$), corresponding to peaks in the velocity distribution at 1000, 1660, 2120, and 2300 m s^{-1}. The $\beta(v)$ parameters also vary considerably between the three spin-orbit states, with different speed components having quite different anisotropies (see the data shown in Table I). It seems unlikely that such highly structured speed distributions and $\beta(v)$ parameters arise exclusively from structure in the rotational state distributions of the CO cofragments. The S($^3P_1$) and S($^3P_0$) products, in particular, are likely to be accompanied by some vibrationally excited CO cofragments, as discussed further below.

Suzuki *et al.* have presented ion images corresponding to the three spin-orbit states for the S(^3P_J) products following dissociation at 223 nm.[11] The speed distributions extracted by means of Abel inversion show somewhat less variation between the spin-orbit states and are less structured than the present data at 248 nm. For the major products born in $J=2$, Suzuki and co-workers[10,11] also reported a velocity-averaged value of the translational anisotropy for the main feature, $\beta \sim 1.1$, which is quite similar to the value observed here (see Table I). However, in the same work[11] the authors also presented a β parameter of 0.2 for the faster fragments observed around 2250 m s^{-1}, which is much smaller than the value obtained here at 248 nm. In their study at a photolysis wavelength of 222 nm, Nan *et al.* reported a speed averaged value of $\beta=0.3$ (Ref. 9) for the $J=2$ products, which again is much smaller than that observed here at longer wavelengths. Alignment effects were not taken into account in these previous studies, which will have had some effect on the values obtained for the translational anisotropy. However, it seems

unlikely that neglect of alignment would make such a big difference to the β parameter in this case, since the alignment observed here is quite small, and the differences are more likely to reflect differences in the dissociation dynamics at the two excitation wavelengths.

In Fig. 9 (middle panel) the speed distributions for the three spin-orbit states are plotted as a function of CO internal energy. The figure also includes vibrational state combs for the bending levels (v_2) of the OCS parent molecule and for the partner CO fragment (v_{CO}). It is apparent from these data, as well as from the $\beta(v)$ parameters shown in Fig. 6, that, in spite of the differences observed between the spin-orbit states, they also share some common features. All three states have a prominent feature in the region of 1580 m s^{-1}, clearly visible as a sharp ring in the images displayed in Figs. 2–4. This is the main feature for S($^3P_2$) products but becomes progressively weaker for S($^3P_1$) and S($^3P_0$). The major S($^3P_2$) products are preferentially generated with a narrow spread of speeds centered around 1580 m s^{-1}, with β=0.93. Although the details of the speed dependence of $\beta(v)$ differ for the three states, a general trend is observed, with small values of β at low speeds increasing to positive values at higher velocity. Note, in particular, that the β parameter at 1580 m s^{-1} is very nearly unity for all three spin-orbit states. A first approximation to the dynamics will need to explain the origins of the feature at 1580 m s^{-1}. Note that at this velocity, the spin-orbit populations are even more nonstatistical than the velocity-averaged values, with S($^3P_2$):S($^3P_1$):S($^3P_0$)$\simeq$20:4:1.

In Fig. 9 the internal energy distributions observed here, shown in the upper panels of the figure, are compared with the analogous distribution observed for the S($^1D_2$) products at 248 nm (Ref. 31) (see the bottom panel of the figure). The sharply peaked feature in the speed distribution around 1580 m s^{-1} for the S(^3P_J) products is similar to those observed for the slow component in the speed distribution of S($^1D_2$) and in the corresponding CO rotational distribution for the singlet channel.[8,11,31,32] If one assumes that CO vibration is not excited following dissociation at 248 nm, then the sharp feature observed in the velocity distribution for the triplet channel at 1580 m s^{-1} would correspond to ~55% of the excess energy being deposited into CO rotation. A detailed simulation of the energy release distribution for J=2 reveals that the feature can be modeled well by a Gaussian CO rotational state population distribution, with a peak at J_{CO}=64 and a full width at half maximum (FWHM) of 9. Combs showing the positions of the various rotational states of the CO coproducts are shown on the speed distributions presented in Fig. 6. If one assumes that excitation occurs preferentially from one quantum in the OCS bending vibration (see further below), then the peak of the distribution would be shifted to J_{CO}=66. These numbers are quite similar to those observed for dissociation to yield S($^1D_2$), particularly for the slow component, which has a peak at J_{CO}=49 (Ref. 31 and a rather narrow distribution.[8,11,31,32] The shift from J_{CO}=49 for the singlet channel to J_{CO}=64 for the triplet channel represents about 35% of the extra 9239 cm^{-1} available energy in the latter case being released into CO rotation, with the rest channeled into translation (see further below).

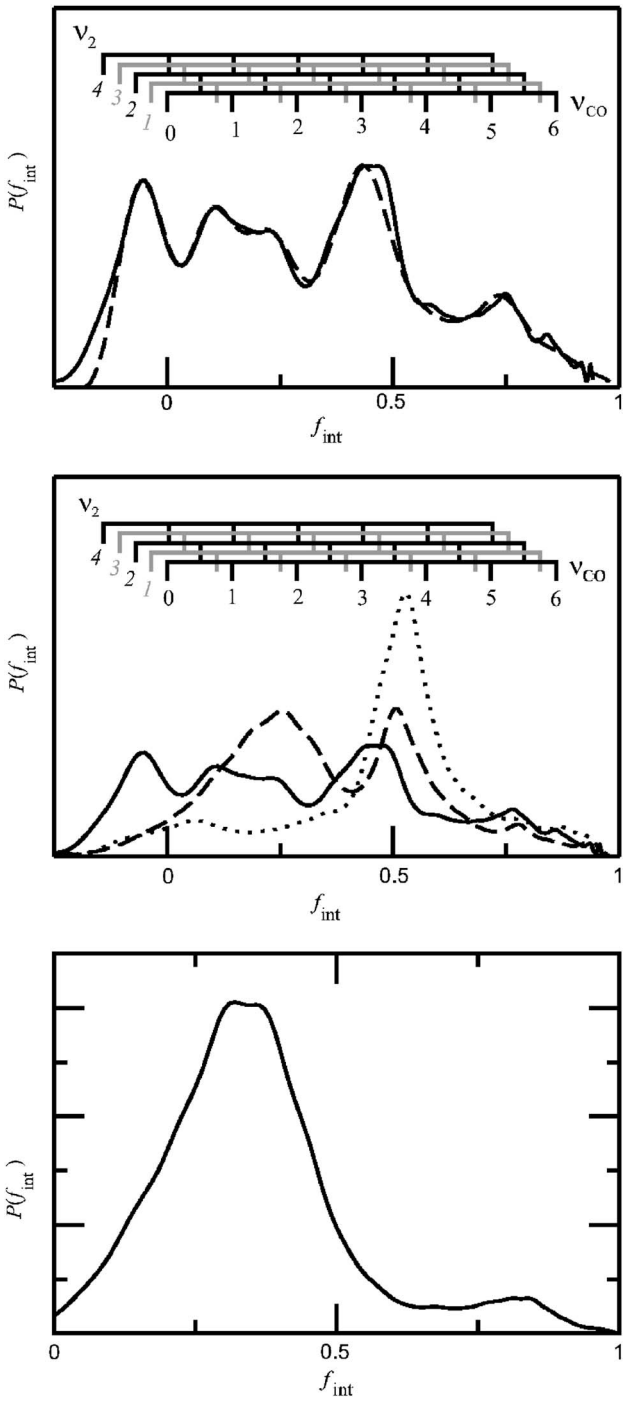

FIG. 9. Top panel Comparison of speed distribution for S($^3P_0$) (——), plotted as a function of rotational energy release, with the results of the simulation (---) described in the text. The CO vibrational populations derived from the simulation for v_{CO}=0–6 are $P(v)$=0.22, 0.18, 0.15, 0.26, 0.06, 0.09, and 0.03. The large population for v=3 arises from fitting the peak around 1580 m s^{-1}, which is believed to originate from another mechanism, leading to rotationally excited CO cofragments. See text for details. The combs show the vibrational states of the bending levels of OCS (v_2) and of the CO products (v_{CO}). Middle panel: Speed distributions for S($^3P_2$) (——), S($^3P_1$) (---), and S($^3P_0$) (···) plotted as a function of rotational energy release. Bottom panel: S($^1D_2$) speed distribution observed at the same dissociation wavelength (Ref. 1). Note that this bottom graph is not plotted on the same abscissa scale as the upper graphs.

For a system with a singlet ground state, triplet products can be generated either following direct excitation into a triplet state, discussed further below, or after intersystem crossing from an optically populated singlet surface. Singlet and triplet states for OCS are illustrated in Fig. 1. The lowest triplet state at linearity is of $^3\Pi$ symmetry and is strongly repulsive in character. It crosses the relevant excited singlet states quite close to the Franck-Condon region, and intersects the ground state at approximately 3 Å. Following excitation to the singlet state [principally the $2\ ^1A'(1\ ^1\Delta)$ state[31]), intersystem crossing could occur directly from the optically prepared state. Given that the $1\ ^3A'(\Pi)$ and $1\ ^3A''(\Pi)$ states are not highly anisotropic and because the crossing between the singlet and triplet states is likely to occur near the Franck-Condon region,[3] which is only slightly displaced from linearity, little rotational excitation is expected in this case. An estimate of the rotational energy release can be made from the values reported for the singlet channel dissociation.[1,11] Dissociation on the $2\ ^1A'$ surface generates singlet products with $\langle f_{\mathrm{rot}}\rangle=0.35$. Assuming that the torque on the departing fragment is imparted primarily before the point of intersystem crossing and that the excess energy beyond this point is deposited principally into translation, the rotational excitation in the resulting triplet products would be $f_{\mathrm{rot}}\sim 0.2$. Note also that a value of β similar to those found for the fast singlet products, $\beta=-0.02$,[1] would be expected from such a mechanism. These estimates do not correspond well with those observed for the main triplet S-atom products born at speeds around 1580 m s^{-1}.

Alternatively, intersystem crossing could occur from the ground $1\ ^1A'$ state to the $1\ ^1A'(^3\Pi)$ state, after part of the product flux initially on the $2\ ^1A'$ surface passes through the conical intersection onto the lowest singlet surface. Potential crossings relevant to this scenario have been identified at near-linear geometries around $R=3$ Å.[2–5] Because a much larger degree of rotational excitation is observed for the singlet fragments dissociating on the ground singlet surface,[11] substantial rotational excitation can be expected to arise from this mechanism. Given that the fragments emerging on the ground singlet surface already posses $J_{\mathrm{CO}}\sim 49$, a relatively minor torque would be required to be exerted on the departing fragments subsequent to the intersystem crossing to excite them to $J_{\mathrm{CO}}\sim 64$. Note also that the β parameter associated with this mechanism is expected to be similar to that observed for the corresponding singlet pathway, i.e., $\beta\sim 1$.[1] Comparison of the experimental data for the singlet and triplet channels suggests that the most likely mechanism leading to triplet products with speeds around 1580 m s^{-1} is this second process, involving excitation into the $2\ ^1A'$ state, followed by non-adiabatic crossing to the ground singlet state, and then finally intersystem crossing to the lowest $1\ ^3A'/1\ ^3A''(1\ ^3\Pi)$ states at $R\sim 3$ Å. We discuss this process further in Sec. IV B.

All three spin-orbit states, but most notably S($^3P_0$) and S($^3P_1$), display evidence for a second triplet production mechanism, responsible for fragments born at speeds other than those yielding the prominent feature at 1580 m s^{-1}. This channel produces a near-statistical distribution of S-atom spin-orbit state populations. Simulations of the internal energy distributions have been undertaken for each of the S-atom spin-orbit states. The clue to the origin of the highly structured CO internal energy distributions is provided by the low-energy features in the S($^3P_0$) distribution (see the simulation shown in the top panel of Fig. 9). For this channel a significant number of products are produced with velocities that exceed the maximum possible for dissociation from the ground vibrational state OCS. These fragments arise from the dissociation of bend-excited OCS parent molecules, similar to previous observations for the S($^1D_2$) product channel.[33] For the S($^3P_0$) products, the corresponding peak in the CO internal energy distribution, shown in the top and middle panels of Fig. 9, occurs at negative energies, since the available energy has been calculated assuming that the OCS precursor is internally cold. This peak, and others at higher CO internal energies, can be modeled satisfactorily in terms of excitation from a range of bending-vibrational levels in OCS in the range $v_2=4-4$, and CO coproduct vibrational levels, $v=0-6$ (see Fig. 9). Good agreement with the S($^3P_0$) distribution can be achieved assuming a single Gaussian rotational distribution centered at $J=26$ with a FWHM=17. Although the modeling shows some (inverse) correlation between the assumed peak in the CO rotational distribution and the value of v_2 required, the structure in the internal energy release distributions is sufficient to conclude that this second production mechanism generates CO products with relatively low levels of rotational excitation, in a range of CO vibrational states. For the S($^3P_0$) products, the simulations suggest the CO vibrational distribution encompasses the full range of energetically accessible levels but is monotonically declining in v_{CO} (see the caption of Fig. 9). Excitation appears to occur preferentially from excited bending levels of OCS. Similar product CO vibrational and rotational distributions provide satisfactory fits to the data for S($^3P_1$) and S($^3P_2$), although the simulations suggest that hot band excitation from excited levels of OCS is less important than that for S($^3P_0$). The simulations also reveal that the vibrational distribution of the CO cofragment increases somewhat with increasing J in the S(^3P_J) atom products.

Two possible mechanisms may give rise to the products born at velocities other than 1580 m s^{-1}. The first is the "direct" intersystem crossing mechanism described above, involving excitation principally into the $2\ ^1A'(1\ ^1\Delta)$ state, followed directly by intersystem crossing at close to linearity onto the $1\ ^3A'/1\ ^3A''(1\ ^3\Pi)$ states. As noted above, this might be expected to generate CO cofragments with relatively low rotational excitation. However, it would seem somewhat surprising that the intersystem crossing process has no effect on the CO rotational excitation at all compared with that generated in the corresponding singlet products, which are born with a most probable $J_{\mathrm{CO}}=30$.[1,11] Note also that the β parameter associated with these fast products in the singlet channel is −0.02, as mentioned above, whereas, for $J=0$ of the triplet channel $\beta\gtrsim 1.0$ (see Table I). An alternative mechanism, mentioned in passing above, might involve direct photon absorption to the $1\ ^3A'/1\ ^3A''(1\ ^3\Pi)$ or the $2\ ^3A''(1\ ^3\Sigma^-)$ states. The $^3\Pi$ state, in particular, should be energetically accessible in the wavelength region of interest.[2–5] At linearity, both transitions would be allowed by

the spin-orbit interaction,[34,35] and, because the selection rule $\Delta\Omega=0, \pm1$ then applies, only $|\Omega|=0$ and $|\Omega|=1$ levels would be expected to be populated significantly on photon absorption. Finally, because the $1\ ^3\Pi$ state is highly repulsive, with only a slight anisotropy in the bending potential,[3] the optically prepared linear excited state would be expected to dissociate rapidly, with little energy being deposited into rotation.

Both of the above scenarios might provide an explanation for why the $S(^3P_0)$ fragments are preferentially generated by hot band excitation. The $^3\Pi_0$ state might be expected to lie higher in energy than the $^3\Pi_1$ and $^3\Pi_2$ states, and thus direct excitation to the former would be enhanced by the extra energy in the OCS bending mode. Note that the wave number of the OCS bending mode, $\omega_e \simeq 520\ cm^{-1}$,[11] is quite close to the $J=2$ to $J=0$ separation in the free S atom.[21] The implication is that the $S(^3P_0)$ products arise preferentially from excitation to, and adiabatic dissociation on, a state with $\Omega=0$, a pathway which would also account for the positive β parameter observed for this channel (see below). In support of this proposition, notice that although the total spin-orbit populations for this dissociation channel are near statistical, some spin-orbit selectivity is observed in the speed distributions and $\beta(v)$ parameters for the three $S(^3P_J)$ levels.

The β parameters for the more statistically distributed S-atom fragments born at velocities other than $1580\ m\ s^{-1}$ also seem to bear out a production mechanism involving direct excitation to a triplet state. In particular, as noted above, the $S(^3P_0)$ products are associated with positive translational anisotropies, particularly at high speeds, in contrast to the fast fragments generated for the singlet channel.[1] These triplet fragments are necessarily born in conjunction with CO in low rotational states and thus are less subjected to the effects of nonaxial recoil than the slow products. The large positive β parameter observed for the fast $S(^3P_0)$ products is suggestive of a parallel transition to either the $1\ ^3\Pi_0$ or $1\ ^3\Sigma_0^-$ states at linearity. The high speed component of $S(^3P_2)$ is also associated with $\beta>0$ at high speeds, which suggests that these products too might arise indirectly from a parallel transition. By contrast, at high velocities the $S(^3P_1)$ products are born with more negative β parameters, consistent with production via a perpendicular transition such as $1\ ^3\Pi_1 \leftarrow 1\ ^1\Sigma_0^+$ or $1\ ^3\Sigma_1^- \leftarrow 1\ ^3\Sigma_0^+$. The velocity dependence of the $\beta(v)$ parameters shown in Fig. 6, particularly for the $J=0$ fragments, which only have a small contribution from the channel centred around $1580\ m\ s^{-1}$, serves to reinforce the argument that the products in question do not arise from excitation to the singlet states responsible for the singlet channel dissociation. For the latter system, the β parameter is close to zero, if not negative at high speeds,[1] tending to greater than unity at low velocities, whereas the triplet channel leading to $J=0$ is characterized by the reverse trend, namely, positive anisotropy at high velocities and near-zero β values at low velocities.

In the recent high resolution study of OCS at a photolysis wavelength of 230 nm, Lipciuc and Janssen found evidence that rotationally excited CO fragments in $J_{CO}=63$ were partnered by spin-orbit *excited* atomic products $S(^3P_0)$.[13] Indeed, inspection of the Abel-inverted ion images for $S(^3P_0)$ obtained here at 248 nm reveals some structure consistent with rotationally excited CO coproducts. These are assumed to originate from the relatively small number of $S(^3P_0)$ products that are formed subsequent to intersystem crossing from the ground state. Interestingly, Lipciuc and Janssen did not find evidence for the major $S(^3P_2)$ products in coincidence with $J_{CO}=63$. If the mechanisms outlined above for 248 nm photodissociation also operate at 230 nm, then the absence of $S(^3P_2)$ lies in the fact that these fragments would be expected to be produced primarily in coincidence with $J_{CO}\sim 75$, rather higher than the $J_{CO}=63$ fragment probed.

B. Angular momentum polarization

In light of the foregoing discussion it would seem sensible to discuss separately the angular momentum polarization for the two mechanisms proposed for $S(^3P_J)$ atom formation. Previously we have employed a prompt recoil, diabatic treatment of the spin-orbit recoupling zone to describe the atomic angular momentum polarization observed for $O(^3P_J)$ generated in the photodissociation of N_2O and SO_2.[18,20,31,36] However, such a treatment is inappropriate in describing the atomic polarization observed here because for both proposed fragmentation pathways there are significant differences between the speed distributions and anisotropy parameters for the three S-atom spin-orbit states. Furthermore, for the main channel, producing fragments at $1580\ m\ s^{-1}$, the spin-orbit populations are also strongly nonstatistical. A diabatic treatment of the spin-orbit coupling zone, in the absence of spin polarization, predicts statistical spin-orbit populations.[18] In the case of the photodissociation of SO_2 at 193 nm, a spin polarized version of the prompt recoil model was also presented,[20] but this too would predict only small deviations of the spin-orbit populations from the statistical limit when the angular momentum polarization is relatively small, as is the case here. The fact that for the present system the speed distributions also differ greatly among the spin-orbit states indicates that spin-orbit coupling cannot simply be "switched on" at large separations, as is assumed in the fast dissociation model. The effect of the spin-orbit interaction must already be substantial at the point where the product flux is transferred onto the triplet surface(s). Such differences in the speed distributions were not observed in previous studies where the diabatic approximation was applied.[18,20]

The reason for the inapplicability of a diabatic treatment of the spin-orbit coupling zone lies in the relative time scales for spin-orbit coupling and traversing the recoupling zone.[37] The velocities of the departing fragments are small compared with other systems to which the spin-unpolarized prompt recoil model has been employed, such as N_2O.[18] Furthermore, the magnitude of the spin-orbit coupling for $S(^3P_J)$ is of the order of $200\ cm^{-1}$, almost twice that of $O(^3P_J)$. The larger spin-orbit coupling in the case of $S(^3P_J)$ implies that the minimum speed at which the diabatic approximation can be safely applied is increased compared to studies involving oxygen atoms. These considerations suggest that the Massey parameter (the ratio of the spin-orbit recoupling time to the

TABLE II. Scattering angle averaged J-state multipoles resolved into the two different speed regimes, as described in the text. See Refs. 18, 20, 22, 31, and 48 for equations for the scattering angle dependence of the molecular frame state multipoles and their scattering angle averages.

	$J=2$		$J=1$	
	ρ_{20}^{mol}	ρ_{22}^{mol}	ρ_{20}^{mol}	ρ_{22}^{mol}
$v\sim 1580$ m s^{-1}	0.096(6)	0.144(15)	−0.021(7)	−0.104(20)
All other velocities	−0.009(2)	0.070(11)	0.195(26)	−0.090(22)

time spent in the recoupling zone) might be as much as six times smaller in the present system than that for N_2O.[18] The prompt recoil model, in which the electron spin is assumed to be unpolarized,[18] predicts that the **J**-polarization parameters for the $J=1$ and $J=2$ spin-orbit states should be of similar magnitude but opposite sign. While this matches the behavior observed here quite well (see Table II), the factors identified above suggest that the application of a diabatic model is unsuitable for this system.

1. An adiabatic model

The main feature in the speed distributions at 1580 m s^{-1} is associated with a highly nonstatistical atomic spin-orbit state distribution, and this channel, in particular, would appear to lend itself more to an adiabatic picture of the dissociation dynamics. However, it is also important to emphasize that these fragments are the ones that are believed to be partnered by highly rotationally excited CO cofragments. For these fragments the effects of nonaxial recoil will be most significant. In the preceding paper[1] it was shown that the observed trends in β parameter with CO rotational state for the singlet channel could be interpreted in terms of excitation to the 2 $^1A'$ state with an in-plane transition moment directed at ~65° to the initial linear axis in OCS, followed by nonaxial recoil leading to large deflection angles for high JCO. Similar arguments apply to the triplet atomic products born around 1580 m s^{-1}. These are believed to be partnered by $J_{CO}\sim 64$, for which we can model β values between 0.5 and 1.0 using values of $R_c=2.5$ Å and $\alpha'=65°$ in the simple model described previously.[1] These values are quite close to those needed to model the velocity-dependent $\beta(v)$ parameters for the singlet channel, following excitation into the 2 $^1A'$ state. Moreover, the calculation suggests that the effects of nonaxial recoil could be very significant for these products.

The correlation diagram for the spin-forbidden dissociation of OCS is illustrated in Fig. 10. As described in Sec. I, two surfaces correlate with triplet product formation at large separations, one of $^3\Sigma^-$ and one of $^3\Pi$ symmetry at linearity. The $^3\Sigma^-$ state lies higher in energy than $^3\Pi$. At shorter range this can be understood in terms of the corresponding orbital occupancy for each state. In the case of the $^3\Sigma^-$ state, the $p_z\equiv p_0$ orbital on the S atom is doubly occupied and points towards the closed shell CO molecule, hence maximizing the exchange repulsion. However, the signs of both the long-range dipole-quadrupole and quadrupole-quadrupole interactions are also consistent with the $^3\Sigma^-$ state lying highest in energy for linear OCS configurations. At long range the molecular states can also be characterized by a total electronic angular momentum projection quantum number Ω. The ordering of the Ω spin-orbit levels at long range has been determined using Hund's rules, consistent with bringing an atom up to a closed shell molecule at linearity. Within these constraints, the value of Ω is equal to M_J, assuming axial recoil. The correlation diagram shown in Fig. 10 is similar to that used by Ausfelder *et al.* to interpret the fine structure populations of OH($^2\Pi$) generated from collisions of O(^3P_J) with hydrocarbons.[38] Finally, upon bending the orbital angular momentum is quenched, and the molecular states descend in symmetry such that $^3\Sigma_0^-$ and $^3\Sigma_1^-$ become $^3A''$, $^3\Pi_{0-}$ becomes $^3A'$, $^3\Pi_{0+}$ transforms as $^3A''$, and $^3\Pi_1$ and $^3\Pi_2$ transform both as $^3A'$ and $^3A''$. These correlations are consistent with those for O(^3P_J)+H_2,[39] bearing in mind the different signs of the quadrupole-quadrupole interaction for that system compared with the present one.[41,40]

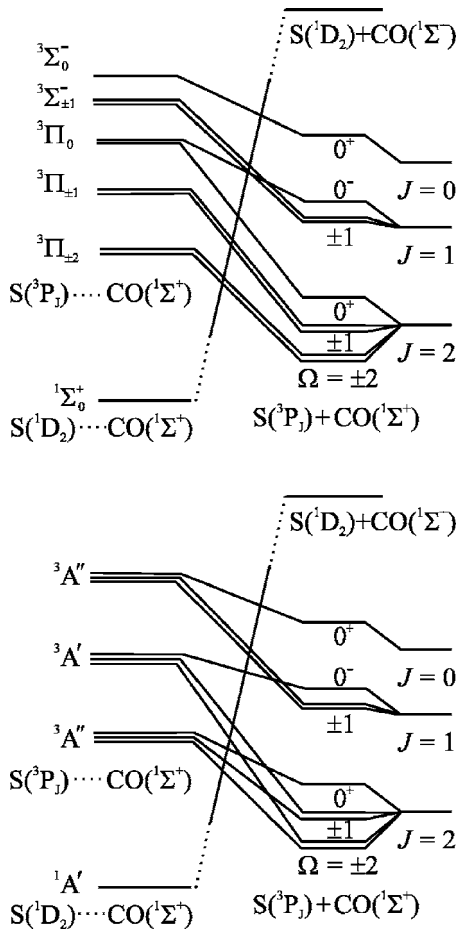

FIG. 10. Adiabatic correlation between atomic and molecular states at linearity (top panel), and for nonlinear configurations (bottom panel). In both cases, the states at long range are labeled according to Ω, which have been ordered on the basis of Hund's rules. At shorter range, the states are ordered according to the expectations based on the long-range interactions (Refs. 20 and 46) and the orbital occupancies. The ground 1 $^1A'$(1 $^1\Sigma^+$) state is included to illustrate the intersystem crossing discussed in the text.

Recall that the main feature in the speed distributions and $\beta(v)$ parameters at 1580 m s^{-1} could be interpreted in terms of intersystem crossing from the ground singlet state onto a surface correlating to triplet products. In the adiabatic limit, product flux on the ground 1 $^1A'$(1 $^1\Sigma^+$) surface would

cross to the lowest $1\,^3A'/1\,^3A''(1\,^3\Pi)$ states, which correlate with $S(^3P_2)$ and $S(^3P_1)$ products, as shown in the lower panel of Fig. 10. By analogy with N_2O,[42,43] we assume that intersystem crossing to the $2\,^3A''(1\,^3\Sigma^-)$ state has a relatively small probability, reflecting a relatively small spin-orbit coupling matrix element with the ground $1\,^1A'(^1\Sigma^+)$ state. The predictions of the adiabatic model for the spin-orbit state populations, at least in nonlinear configurations, are in excellent agreement with the experimental result. If crossing from the $1\,^1A'(1\,^1\Sigma^+)$ to the $1\,^3A'/1\,^3A''(1\,^3\Pi)$ states occurs with near-equal probability, as would appear to be the case in N_2O,[42,43] at nonlinear configurations this model would predict an $S(^3P_J)$ spin-orbit ratio $S(^3P_2):S(^3P_1):S(^3P_0)=5:1:0$, in excellent agreement with the experimental estimate for those fragments born around 1580 m s^{-1} (5: 1: 0.25).

Concerning the angular momentum polarization of the S-atom products born at 1580 m s^{-1}, the adiabatic correlation at nonlinear configurations shown in the lower panel of Fig. 10 predicts an isotropic polarization for the $J=2$ products and a preference for population of $M_J=0$ in the case of $J=1$. This is broadly consistent with experimental observation (see Fig. 8). The slightly diminished population of the $M_J=0$ component of the $J=2$ level might arise if the crossing from the $1\,^1A'(1\,^1\Sigma^+)$ to the $1\,^3A'/^3A''(1\,^3\Pi)$ showed a modest bias in favor of the $1\,^3A'$ state. However, the rather weak polarization observed for the $J=1$ products is not well accounted for by the adiabatic model. These arguments, of course neglect any consideration of nonaxial recoil, but it is possible that because the polarization predicted here is determined in the exit channel by the long-range adiabatic correlations, the effects of nonaxial recoil might be less important in this case.

The mechanism proposed here is consistent with the known mechanism for the production of "slow" singlet fragments. Calculations by Suzuki *et al.* for this channel[11] indicate that singlet products emerge from the conical intersection onto the ground electronic state surface with a large degree of motion in the bending coordinate. As the adiabaticity of the crossing with the triplet surfaces is determined by the energy separation of the latter states and by the speed of crossing (much in the same way as crossing the spin recoupling zone), a wave packet whose motion is primarily in the bend coordinate on the singlet surface will reach the crossing region with small transverse velocity, thus potentially favoring adiabatic behavior. The mechanism proposed here for the production of $S(^3P_J)$ products following 248 nm photodissociation of OCS is also quite similar to that proposed for the collisional quenching of $S(^1D_2)$ to $S(^3P_J)$ by CO.[3–5]

Although an adiabatic picture at nonlinear configurations seems to describe satisfactorily several of the experimental findings associated with the main feature at 1580 m s^{-1}, the analogous correlation at linear configurations (see the upper panel in Fig. 10) fails to account for the present results. Under these circumstances the spin-orbit interaction might be expected to couple states of the same Ω quantum number most strongly as that of the ground singlet state, namely, $\Omega=0$. Thus, if dissociation took place exclusively at linearity, the adiabatic correlation would predict equal spin-orbit state populations and exclusive population of the $M_J=0$ sublevels, at variance with the experiments. (In fact, if one also imposes parity conservation one would expect preferential population of the $J=0$ and 2 components at linear configurations.) However, dissociation leading to the S-atom products in question has been shown in the previous section to be most likely correlated with highly rotationally excited CO cofragments, and thus dissociation from collinear configurations seems highly unlikely.

TABLE III. Scattering angle averaged L-state multipoles averaged over all velocities, apart from the component at 1580 m s^{-1}. The L-state multipoles have been calculated using the spin-unpolarized fast-dissociation model described elsewhere Refs. 18, 20, 22, and 31.

$J=2$		$J=1$	
ρ_{20}^{mol}	ρ_{22}^{mol}	ρ_{20}^{mol}	ρ_{22}^{mol}
0.003(1)	0.068(11)	−0.217(30)	0.102(26)

For products that are not born in the main peak of the speed distribution at 1580 m s^{-1}, the polarization behavior is quite different. These fragments appear to be born with lower degrees of CO cofragment rotational excitation, and therefore the complicating effects of nonaxial recoil are probably less important for these fragments. The spin-orbit populations in this channel are more statistical, although differences between the speed distributions of the three spin-orbit states are clearly observed. It would appear that these products do not conform well to either the adiabatic or diabatic limits discussed above. If the spin-unpolarized fast dissociation model[18] is used to interpret the $\boldsymbol{J}$-polarization data (see Table II) for this velocity subset, the $\boldsymbol{L}$ polarization obtained (see Table III) is found to be quite different for $J=1$ and $J=2$, suggesting either that the spin *is* polarized or that the fast dissociation model provides an inappropriate treatment of the products not born around 1580 m s^{-1}. Given the differences in speed distribution between the spin-orbit states, it would seem that the latter explanation is the more likely. A reasonable starting point for interpreting the polarization observed in this channel is to consider the adiabatic correlations at linearity (see the top panel in Fig. 10). In the adiabatic limit, the preference for $M_J=\pm1$ for $J=1$ fragments is consistent with dissociation on the $1\,^3\Sigma_1^-$ state at linearity. This component of the $1\,^3\Sigma_1^-$ state could be populated by a direct perpendicular transition from the ground state, consistent with the more negative β values associated with the $J=1$ fragments at velocities other than 1580 m s^{-1}. Similarly, parallel excitation to the $1\,^3\Sigma_0^-$ component, followed by adiabatic dissociation to S-atom fragments with $J=0$ might explain the positive β parameter observed for this channel. However, such an adiabatic mechanism does not also account for the significant population of $S(^3P_2)$ products observed experimentally in this velocity regime. Furthermore, direct excitation to, and dissociation on, the $1\,^3\Pi_0$ and $1\,^3\Pi_1$ states at linearity might seem to be the more likely candidates on energetic and Franck-Condon grounds for the states accessed directly by photon absorption (see Sec. IV A). Unfortunately, it is difficult to see how the $^3\Pi$ states could generate the spin-orbit

populations and angular momentum polarizations observed experimentally for the S atoms born in this speed regime. It is possible that a partially adiabatic model, in which the Ω quantum number is conserved in the exit channel,[38] might do a better job in describing the spin-orbit populations and polarization parameters, but in the absence of more detailed information about the triplet state potential energy surfaces of OCS we have not investigated this possibility further.

2. Summary of proposed mechanism

Triplet product formation following excitation from a singlet ground state can arise either by direct optical excitation to a triplet surface or by intersystem crossing from an initially excited singlet surface. Similarities in the speed distributions and β parameters reported for this channel with those observed in the preceding paper[1] for S($^1D_2$) product formation suggest that the majority of triplet products formed in a narrow range of S-atom velocities around 1580 m s^{-1} are generated by intersystem crossing from the ground singlet $1\,^1A'$ surface. These triplet products have properties that match closely the minor singlet channel pathway involving the conical intersection between the optically accessed $2\,^1A'$ and the ground state, as previously identified by Suzuki *et al.*[11] It is proposed that part of this product flux on the ground singlet surface undergoes intersystem crossing with the lowest triplet $1\,^1A'/1\,^1A''(1\,^3\Pi)$ surfaces at $R \simeq 3$ Å. A simple adiabatic model has been used to interpret the reported spin-orbit populations and polarization parameters and provides some support for the proposed mechanism. The mechanism is also consistent with a triplet quantum yield of around 5%.[9] The yield of slow S($^1D_2$) atoms within the first absorption band is between 17% and 24%. As not all product flux on the ground state is expected to undergo intersystem crossing, it follows that the overall triplet quantum yield should only be small.

Products formed at velocities other than around the main 1580 m s^{-1} feature have been shown to arise from a different mechanism, most likely involving direct excitation to a triplet state. These products appear to be formed with relatively little CO rotational excitation, but significant vibrational excitation, suggesting excitation to a state with a preferred linear geometry. The β parameter data suggest Ω-conserving dissociation subsequent to parallel and perpendicular excitations into states with $\Omega=0$ and ±1, respectively. The spin-orbit populations and polarization parameters are more difficult to interpret but somewhat favor direct excitation to the $1\,^3\Sigma^-$ state, although the participation of the $1\,^3\Pi$ state seems more likely on Franck-Condon and energetic grounds.

C. Comparison with N_2O

We have previously reported a study of the triplet dissociation channel in N_2O at 193 nm.[18] The reported spin-orbit state specific speed distributions and β parameters were similar to each other and to those previously found for the singlet channel.[44,45] This was taken to indicate that similar geometries were accessed upon photoabsorption, with population subsequently undergoing intersystem crossing from the excited singlet state to a nearby triplet state. Nonzero alignment parameters were obtained for both the O($^3P_1$) and O($^3P_2$) atomic products. Fast dissociation models were successfully applied to the interpretation of these data,[18,31] indicating that dissociation was rapid on the time scale of the spin-orbit interaction and that the spin angular momentum during dissociation is largely unpolarized. The extracted orbital angular momentum L was preferentially aligned perpendicular to the recoil velocity, with preferential population of $M_L=0$. This finding was interpreted in terms of dissociation products being primarily generated on the $2\,^3A''(1\,^3\Sigma^-)$ state.[18] Subsequent application of the long-range interaction model, similar to that applied to the singlet channel of N_2O (Ref. 46) and to SO_2,[20] suggested, however, that the polarization data might also be compatible with the involvement of the $1\,^3A''(1\,^3\Pi)$ state.[31]

At first sight, the picture of the triplet channel arising from the photodissociation of N_2O (Ref. 18) appears to be quite different to the one given here for OCS. In the case of N_2O, where the quantum yield of the triplet channel is only 0.005,[47] there is no evidence for intersystem crossing from the ground $1\,^1A'(1\,^1\Sigma^+)$ state to the lowest triplet $1\,^3A'/1\,^3A''(1\,^3\Pi)$ state, which we suggest provides the main mechanism for triplet channel formation in OCS. In OCS this mechanism requires initial excitation to the $2\,^1A'$ state followed by internal conversion to the ground state, a process which has not been observed in the singlet channel of N_2O. In the latter case, if singlet flux does not cross to the ground state, then of course the intersystem crossing channel from the ground state would be switched off. The triplet formation mechanism in N_2O appears more similar to the minor formation channel in OCS, namely, that involving direct excitation to either the $2\,^1A''(^3\Sigma^-)$ or $1\,^3A'/1\,^3A''(1\,^3\Pi)$ states. In the case of OCS, the $1\,^3\Pi$ state appears to be much closer to the Franck-Condon region at the wavelengths associated with the first absorption band, and this makes direct excitation into this state rather more likely than in N_2O.

V. CONCLUSIONS

We have reported speed distributions, translational anisotropies, and atomic angular momentum polarization parameters for the S(^3P_J) products of the 248 nm photodissociation of OCS. The speed distributions and β parameters were found to be in broad agreement with the few values reported previously for excitation into the first absorption band. Angular momentum polarization was characterized for the first time for this system. Interpretation of these data in terms of an adiabatic model has allowed a likely dissociation pathway to be identified for the main dissociation products born around 1580 m s^{-1}. Optical excitation to the $2\,^1A'$ surface is thought to constitute the first step, as for the singlet channel dissociation. This is followed by crossing via a conical intersection to the ground $1\,^1A'$ state, from which preferential population of the $^3A'/^3A''(^3\Pi_2)$ states occurs via intersystem crossing. The proposed mechanism provides a rationale for the observed spin-orbit populations, speed distributions, translational anisotropy parameters, and atomic angular momentum polarization, as well as the S(^3P_J)-atom quantum yield. The remainder of the S(^3P_J) products, which

are born at speeds other than 1580 m s^{-1}, could be interpreted as arising from direct excitation into a triplet state. However, the data for these fragments, which do not appear to fit well with either the diabatic or adiabatic limits, are harder to interpret. The present limited information about the potential energy surfaces for the triplet states, together with the lack of studies of this channel at different wavelengths, means that a number of features observed here have been left unexplained. It is hoped that the present findings will encourage further experimental and theoretical studies on this dissociation pathway in the future.

ACKNOWLEDGMENTS

The authors gratefully acknowledge the EPSRC for research grants. The authors gratefully acknowledge helpful discussions with Professor O.S. Vasyutinskii (Ioffe Institute, St. Petersburg).

[1] M. Brouard, A. V. Green, F. Quadrini, and C. Vallance, J. Chem. Phys. **127**, 084304 (2007).
[2] J. Hijazo, M. Gonzáles, R. Sayós, and J. J. Nova, Chem. Phys. Lett. **222**, 15 (1994).
[3] Y. Inagaki, M. Abe, Y. Matsumi, M. Kawasaki, and H. Tachikawa, J. Phys. Chem. **99**, 12822 (1995).
[4] H. Tachikawa, J. Chem. Phys. **108**, 3966 (1998).
[5] H. Tachikawa, T. Hamabayashi, and M. Igarashi, J. Mol. Struct. **453**, 191 (1998).
[6] G. Nan, D. W. Neyer, P. L. Houston, and I. Burak, J. Chem. Phys. **98**, 4603 (1993).
[7] N. Sivakumar, I. Burak, W. Y. Cheung, P. L. Houston, and J. W. Hepburn, J. Phys. Chem. **89**, 3609 (1985).
[8] N. Sivakumar, G. E. Hall, P. L. Houston, J. W. Hepburn, and I. Burak, J. Chem. Phys. **88**, 3692 (1988).
[9] G. Nan, I. Burak, and P. L. Houston, Chem. Phys. Lett. **209**, 383 (1993).
[10] H. Katayanagi, Y. Mo, and T. Suzuki, Chem. Phys. Lett. **247**, 571 (1995).
[11] T. Suzuki, H. Katayanagi, S. Nanbu, and M. Aoyagi, J. Chem. Phys. **109**, 5778 (1998).
[12] A. Sugita, M. Mashino, M. Kawasaki, Y. Mastumi, R. Bersohn, G. Trottkriegeskort, and K. H. Gericke, J. Chem. Phys. **109**, 5778 (1998).
[13] M. L. Lipciuc and M. H. M. Janssen, Phys. Chem. Chem. Phys. **8**, 3007 (2006).
[14] A. T. J. B. Eppink and D. H. Parker, Rev. Sci. Instrum. **68**, 3477 (1997).
[15] D. W. Chandler and P. L. Houston, J. Chem. Phys. **87**, 1445 (1987).
[16] M. Bass, M. Brouard, A. P. Clark, and C. Vallance, J. Chem. Phys. **117**, 8723 (2002).
[17] M. J. Bass, M. Brouard, A. P. Clark, B. Martínez-Haya, and C. Vallance, Phys. Chem. Chem. Phys. **5**, 856 (2003).
[18] M. Brouard, A. P. Clark, C. Vallance, and O. S. Vasyutinskii, J. Chem. Phys. **119**, 771 (2003).
[19] B. Martínez-Haya, M. J. Bass, M. Brouard, C. Vallance, I. Torres, and J. Barr, J. Chem. Phys. **120**, 11042 (2004).
[20] M. Brouard, R. Cireasa, A. P. Clark, T. J. Preston, C. Vallance, G. C. Groenenboom, and O. S. Vasyutinskii, J. Phys. Chem. A **108**, 7965 (2004).
[21] *NIST Atomic Spectra Database*, http://physics.nist.gov/PhysRefData/ASD/index.html (Version 3, 2005).
[22] M. Brouard, R. Cireasa, A. P. Clark, G. C. Groenenboom, G. Hancock, S. J. Horrocks, F. Quadrini, G. A. D. Ritchie, and C. Vallance, J. Chem. Phys. **125**, 133308 (2006).
[23] A. G. Smolin, O. S. Vasyutinskii, E. R. Wouters, and A. G. Suits, J. Chem. Phys. **121**, 6759 (2004).
[24] Y. Mo, H. Katayanagi, M. C. Heaven, and T. Suzuki, Phys. Rev. Lett. **77**, 830 (1996).
[25] M. C. G. N. van Vroonhoven and G. C. Groenenboom, J. Chem. Phys. **116**, 1965 (2002).
[26] C. W. Hsu, C. L. Liao, Z. X. Ma, P. J. H. Tjossem, and C. Y. Ng, J. Chem. Phys. **92**, 6283 (1992).
[27] W. B. Tzeng, H. M. Yin, W. Y. Leung, J. Y. Luo, S. Nourbakhsh, G. D. Flesch, and C. Y. Ng, J. Chem. Phys. **88**, 1658 (1988).
[28] I. M. Waller and W. J. Hepburn, J. Chem. Phys. **87**, 3261 (1987).
[29] M. P. de Miranda and F. J. Aoiz, Phys. Rev. Lett. **93**, 083201 (2004).
[30] M. P. de Miranda, F. J. Aoiz, V. Saez-Rabanos, and M. Brouard, J. Chem. Phys. **121**, 9830 (2004).
[31] A. P. Clark, R. Cireasa, M. Brouard, F. Quadrini, and C. Vallance, in *Molecular Reaction and Photodissociation Dynamics in the Gas Phase*, edited by P. D. Kleiber and K. C. Lin (Research Signpost, India, in press).
[32] A. J. van den Brom, T. P. Rakitzis, J. van Heyst, T. N. Kitsopolous, S. R. Jezowki, and M. H. M. Janssen, J. Chem. Phys. **117**, 4255 (2002).
[33] M. H. Kim, W. Li, S. K. Lee, and A. G. Suits, Can. J. Phys. **82**, 880 (2004).
[34] G. Herzberg, *Molecular Spectra and Molecular Structure. I. Spectra of Diatomic Molecules* (Van Nostrand, Princeton, 1959).
[35] G. Herzberg, *Molecular Spectra and Molecular Structure. III. Electronic Spectra and Electronic Structure of Polyatomic Molecules* (Van Nostrand, Princeton, 1967).
[36] A. P. Clark, M. Brouard, F. Quadrini, and C. Vallance, Phys. Chem. Chem. Phys. **8**, 5591 (2006).
[37] H. S. W. Massey, Rep. Prog. Phys. **12**, 248 (1948).
[38] F. Ausfelder, H. Kelso, and K. G. McKendrick, Phys. Chem. Chem. Phys. **4**, 473 (2002).
[39] S. Atahan, J. Klos, P. S. Zuchowski, and M. H. Alexander, Phys. Chem. Chem. Phys. **8**, 4420 (2006).
[40] D. B. Lawson and J. F. Harrison, J. Phys. Chem. A **101**, 4781 (1997).
[41] A. D. Buckingham, Adv. Chem. Phys. **12**, 107 (1967).
[42] A. H. H. Chang and D. R. Yarkony, J. Chem. Phys. **99**, 6824 (1993).
[43] T.-S. Chu, T.-X. Xie, and K.-L. Han, J. Chem. Phys. **121**, 9352 (2004).
[44] T. F. Hanisco and A. C. Kummel, J. Phys. Chem. **97**, 7242 (1993).
[45] D. W. Neyer, A. J. R. Heck, and D. W. Chandler, J. Phys. Chem. **110**, 3411 (1999).
[46] J. M. Teule, G. C. Groenenboom, D. W. Neyer, D. W. Chandler, and M. H. M. Janssen, Chem. Phys. Lett. **320**, 177 (2000).
[47] S. Nishida, K. Takahashi, Y. M. N. Taniguchi, and S. Hayashida, J. Phys. Chem. A **108**, 2451 (2004).
[48] A. S. Bracker, E. R. Wouters, A. G. Suits, and O. S. Vasyutinskii, J. Chem. Phys. **110**, 6749 (1999).